

# Active Contour Segmentation with Affine Coordinate-Based Parametrization

Q. Xue<sup>1,2</sup>, L. Igual<sup>1</sup>, A. Berenguel<sup>1</sup>, M. Guerrieri<sup>3</sup>, L. Garrido<sup>1</sup>

<sup>1</sup>*Departament de Matemàtica Aplicada i Anàlisi, Universitat de Barcelona, Barcelona, Spain*

<sup>2</sup>*Department of Mathematics, Tongji University, Shanghai, China*

<sup>3</sup>*Departament d'Informàtica i Matemàtica Aplicada, Universitat de Girona, Girona, Spain*

*xueqi.bhlt@gmail.com, ligual@ub.edu, abcworld22@gmail.com, mariteg@ima.udg.edu, lluis.garrido@ub.edu*

Keywords: Active Contours, Affine Coordinates, Mean Value Coordinates

Abstract: In this paper, we present a new framework for image segmentation based on parametrized active contours. The contour and the points of the image space are parametrized using a set of reduced control points that have to form a closed polygon in two dimensional problems and a closed surface in three dimensional problems. By moving the control points, the active contour evolves. We use mean value coordinates as the parametrization tool for the interface, which allows to parametrize any point of the space, inside or outside the closed polygon or surface. Region-based energies such as the one proposed by Chan and Vese can be easily implemented in both two and three dimensional segmentation problems. We show the usefulness of our approach with several experiments.

## 1 INTRODUCTION

Active contours have been proved to be a powerful tool for segmentation in image processing. In active contours an evolving interface is propagated in order to recover the shape of the object of interest. In a two dimensional problem, the evolving interface is a contour whereas in a three dimensional problem the evolving interface is a surface. The interface is evolved by minimizing an energy that mathematically expresses the properties of the object to be segmented. In this energy functional, the terms corresponding to image features can be either edge-based and/or region-based. Edge-based terms measure features on the evolving interface to identify object boundaries and are usually based on a function of the image gradient (Caselles et al., 1997). They are known to be sensitive to noise and thus energies based on such type of features usually need the evolving interface to be initialized near the solution.

Region-based terms were introduced by Chan and Vese (Chan and Vese, 2001). In this case some features that are measured inside and outside of the regions allows to evolve the interface and thus drive the energy to its minimum. Chan and Vese minimize the variance of the gray-level in the interior and exterior regions. Region-based terms are known to be more robust to noise than edge-based terms and

thus they usually do not need the initialization to be near the solution. Since the work of Chan and Vese other approaches have extended the idea by measuring other types of features (Rousson and Deriche, 2002; Michailovich et al., 2007). However, the latter approaches do measure the features in the whole inner and outer regions and thus may fail if these features are not spatially invariant. This problem has been tackled in (Lankton and Tannenbaum, 2008), in which the inner and outer regions are defined by means of a band around the evolving interface. Thus, their approach is suited for segmenting objects having heterogeneous properties.

Depending on the representation of the evolving interface, active contours may be classified into parametric or geometric ones. In parametric approaches the interface in two dimensional problems may be described by means of a set of discrete points (Kass et al., 1988) or using basis functions such as B-splines (Jacob et al., 2004). In three dimensional problems, parametrizations using B-Splines (Barbosa et al., 2012) have also been used. In general, using basis functions such as B-splines allows to use less parameters to represent the curve than directly discretizing the curve or surface and have inherent regularity and hence do not require additional constraints to ensure smoothness. Parametric contours are able to deal easily with edge-based energies. However,

dealing with region-based energies is more difficult, see (Jacob et al., 2004; Barbosa et al., 2012) for instance. Moreover, parametric approaches require the user to define the number of control points that will be used to evolve the contour and it is difficult to deal with topological changes. This has favored that many works have been tackled using geometric approaches.

Geometric approaches represent the evolving interface as the zero level set of a higher dimensional function, which is usually called level set function. Therefore geometric approaches are also called level set approaches. Level set approaches are able to cope with the change of the curve topology and thus are able to segment multiple unconnected regions. This property has made level sets very popular approaches. However, level set approaches are usually computationally more complex and difficult to deal with since they increase the dimension of the problem by one. This makes level sets a difficult approaches in three-dimensional applications which are common in medical image segmentation.

In this paper, we focus on parametric representations due to its computational advantages and simplicity. A direct consequence of the explicit formulation is the loss of topological flexibility. However, this limitation is a mild constraint in many applications, where the goal may be to simply segment one connected object and thus the topological flexibility of the level sets is not needed.

We contribute with a novel framework for segmenting two and three dimensional connected objects using a new class of parametric active contours. The parametrization is based on a class of deformable models well known in computer graphics such as the animation of characters for video games or movies. Such models are usually made up of millions of triangles. The motion of the character is controlled by a reduced number of control points: when these control points move the associated character deforms accordingly. A similar idea is applied in our paper: the evolving interface, the interior and exterior regions are parametrized by a set of control points. When these control points move the interface evolves correspondingly to the object to be segmented.

Our work stems from the ideas of free-form deformations (Faloutsos et al., 1997; Coquillart, 1990). Free-form deformations have been actively used for medical image registration (Rueckert et al., 1999). However, to the best of our knowledge, free-form deformations have not been used for parametric active contours. In our work we use the *mean value coordinates* as the parametrization tool for the evolving interface (Floater, 2003). Mean value coordinates have several advantages over free-form deformation,

namely that control points only need to form a closed polygon in two dimensional problems (or surface in three dimensional problems) that may have any shape. Any point of the space, inside or outside of this polygon (or surface), can be parametrized with respect to the control points. For free-form deformations the control points need to form a regular shape and only interior points can be parametrized.

The rest of the paper is organized as follows: Section 2 reviews the related state-of-the-art work. Section 3 introduces the proposed segmentation method. Section 4 gives the implementation details. Section 5 shows the experimental results. Finally, Section 6 concludes the paper.

## 2 RELATED WORK

In this Section, we review the state-of-the-art literature in level set techniques and computer graphic techniques related to our work.

### 2.1 Active Contours

The classic method of segmentation of Kass et al. (Kass et al., 1988) minimizes the following energy

$$E(C) = \alpha \int_0^1 \|C'(p)\|^2 dp + \beta \int_0^1 \|C''(p)\|^2 dp - \lambda \int_0^1 \|\nabla I(C(p))\| dp. \quad (1)$$

where  $C(p) : [0, 1] \rightarrow R^2$  is an Euclidean parametrization of the evolving interface and  $I : R^2 \rightarrow R$  is the gray level image. As commented previously two different approaches may be used to represent  $C$ , namely *parametric active contours* and *level sets*. The former is based on directly discretizing the curve  $C$  by means of a set of points and letting these points evolve independently. The level set methods are based on embedding the curve  $C$  in a higher dimensional function  $\phi$  which is defined over all the image. Instead of evolving the curve  $C$ , the function  $\phi$  is evolved. The curve  $C$  corresponds to the zero level curve of  $\phi$ .

Rather than only using information on the interface, Chan and Vese proposed a method to evolve a curve by minimizing the variance in the interior region,  $\Omega_1$ , and exterior region,  $\Omega_2$ , defined by  $C$  (Chan and Vese, 2001), see Figure 4. The energy the authors minimize is

$$E(C) = \frac{1}{2} \iint_{\Omega_1} (I - \mu_1)^2 dx dy + \frac{1}{2} \iint_{\Omega_2} (I - \mu_2)^2 dx dy, \quad (2)$$

where the original terms based on the contour length and area of  $\Omega_1$  have been dropped for simplicity. In Equation (2), the image  $I : R^2 \rightarrow R$  corresponds to the observed data. The  $\mu_1$  and  $\mu_2$  refer to mean intensity values in the interior and exterior regions, respectively. In order to minimize the previous energy, authors use a level set method. They first compute the corresponding Euler-Lagrange equations and then discretize the evolution equations. The successive iterations of the evolution equations allows to evolve  $\phi$  and thus the interface  $C$ .

## 2.2 Mean Value Coordinates

An important problem in computer graphics is to define an appropriate function to linearly interpolate data that is given at a set of vertices of a closed contour or surface. Such interpolants can be used in applications such as parametrization, shading or deformation. The latter application is our main interest in this work and thus we will discuss it next. In this section we will first focus on the two dimensional case and afterwards we will discuss some details regarding the extension to the three dimensional case.

Gouraud (Gouraud, 1971) presented a method to linearly interpolate the color intensity at the interior of a triangle given the colors at the triangle vertices. Assume the triangle has vertices  $\{\mathbf{v}_1, \mathbf{v}_2, \mathbf{v}_3\}$  and corresponding color values  $\{f_1, f_2, f_3\}$ . The color value of an interior point  $\mathbf{p} = (x, y)$  of this triangle can be computed as follows

$$\hat{f}[\mathbf{p}] = \frac{\sum_j w_j f_j}{\sum_j w_j}, \quad (3)$$

where  $w_j$  is the area of the triangle given by vertices  $\{\mathbf{p}, \mathbf{v}_{j-1}, \mathbf{v}_{j+1}\}$ .

Many researchers have used these type of interpolants for mesh parametrization methods (Hormann and Greiner, 2000; Floater, 2003)) as well as free-form deformation methods (Coquillart, 1990) among others. Both applications require that a point  $\mathbf{p}$  be represented as an *affine combination* of the vertices of an closed contour given by vertices  $\mathbf{v}_i$ :

$$\mathbf{p} = \frac{\sum_i w_i \mathbf{v}_i}{\sum_i w_i}, \quad (4)$$

and we say that the coordinate function

$$\frac{w_i}{\sum_j w_j} \quad (5)$$

is the corresponding *affine coordinate* of the point  $\mathbf{p}$  with respect to the vertices  $\mathbf{v}_i$ .

A wealth of approaches have been published for the computation of the affine coordinates  $w_i$ . We may

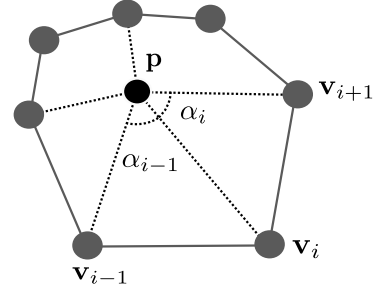


Figure 1: For a given point  $\mathbf{p}$ , the mean value coordinate associated to point  $\mathbf{v}_i$  is computed using  $\mathbf{v}_i$ ,  $\mathbf{v}_{i-1}$  and  $\mathbf{v}_{i+1}$ .

mention those that have interest for deformation applications, namely mean value coordinates (Floater, 2003), positive mean values coordinates (Lipman et al., 2007), harmonic coordinates (Joschi et al., 2007) or Green coordinates (Lipman et al., 2008). Among them, the mean value coordinates are easy to compute and therefore we have selected them in our work.

*Mean value coordinates* were initially proposed for mesh parametrization problems (Floater, 2003). The author demonstrated that the interpolation generated smooth coordinates for any point  $\mathbf{p}$  inside the kernel of a star-shaped polygon. Later on, in (Hormann and Floater, 2006) it was demonstrated that mean value coordinates extended to any simple planar polygon and to any point  $\mathbf{p}$  of the plane.

Assume the set of vertices  $\mathbf{v}_j$ ,  $j = 1 \dots N$ , of a simple closed polygon, is given. For a point  $\mathbf{p} \in R^2$ , its mean value coordinates  $\phi_i(\mathbf{p})$  are computed as

$$\phi_i(\mathbf{p}) = \frac{w_i}{\sum_{j=1}^N w_j} \quad i = 1 \dots N, \quad (6)$$

where

$$w_i = \frac{\tan(\alpha_{i-1}/2) + \tan(\alpha_i/2)}{\|\mathbf{v}_i - \mathbf{p}\|}, \quad (7)$$

and  $\|\mathbf{v}_i - \mathbf{p}\|$  is the distance between the vertex  $\mathbf{v}_i$  and  $\mathbf{p}$ , and  $\alpha_i$  is the *signed* angle of  $[\mathbf{v}_i, \mathbf{p}, \mathbf{v}_{i+1}]$ , see Figure 1.

Given the affine coordinates  $\phi_i(\mathbf{p})$  of a point  $\mathbf{p}$ , the point  $\mathbf{p}$  can be recovered with

$$\mathbf{p} = \sum_{i=1}^N \phi_i(\mathbf{p}) \mathbf{v}_i. \quad (8)$$

If the vertices  $\mathbf{v}_i$  of the polygon move to positions  $\mathbf{v}'_i$ , the “deformed” point  $\mathbf{p}'$  can be recovered as

$$\mathbf{p}' = \sum_{i=1}^N \phi_i(\mathbf{p}) \mathbf{v}'_i, \quad (9)$$

see Figure 2.

For a given a set of points  $\{\mathbf{p}\}$  the affine coordinates are computed in an independent way for each

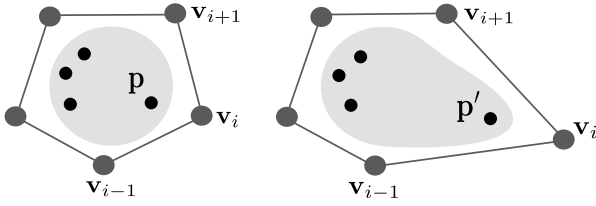


Figure 2: Example of the deformation of a region by means of a closed polygon. From left to right: a polygon vertex  $v_i$  is moved producing the consequent deformation of the region after applying the interpolation function. Pixels near the moved vertex  $v_i$  are affected more than pixels farther away due to the distance in the denominator of Equation (7).

point as described in this section. If a point  $v_i$  of the polygon is stretched in a particular direction, all the points  $\{\mathbf{p}\}$  follow the same direction with an associated weight given by  $\varphi_i(\mathbf{p})$ . The points  $\mathbf{p}$  that are near the moved vertex have higher weights (see denominator of Equation (7)) and thus suffer a larger “deformation” than the points which are farther away. Figure 2 and Figure 3 show an example to illustrate this phenomena. In Figure 2 we schematically show how a cloud of points can be deformed if one of the polygon vertices is moved. Figure 3 depicts the influence of the polygon vertex distance to a curve. In this example mean value coordinates have been used to represent the curve with respect the closed polygon. On the left column, the initial configurations are shown. The polygon, made up of 16 vertices, is shown with a solid line whereas the curve to deform with a dashed line. From top to bottom, different initializations for the polygon are shown: the first two rows are associated to polygon outside the curve whereas the last row is associated to a polygon inside the curve. The second and third column show how the curve is deformed when a control point of the polygon is moved. As can be seen, the movement of the polygon produces a smooth deformation of the curve. The closer the polygon to the curve, the higher the deformation is applied to the curve.

In the three dimensional case a point  $\mathbf{p}$  will be described with respect to a closed surface made up of triangles with vertices  $v_i$ . The algorithm to compute the mean value coordinates  $\varphi_i(\mathbf{p})$  for a point  $\mathbf{p} \in R^3$  is described in (Ju et al., 2005). However, we would like to point out here that Equations (6) and (9) are still valid in the three dimensional case. Thus, it is relatively easy to extend any two dimensional method to the three dimensional case.

Equations (6) and (9) are the basis for the methods we have developed in our work. The closed polygon or surface can be interpreted as a cage that encloses the object to deform. In the context of our work, the control points are the cage vertices. The interior and

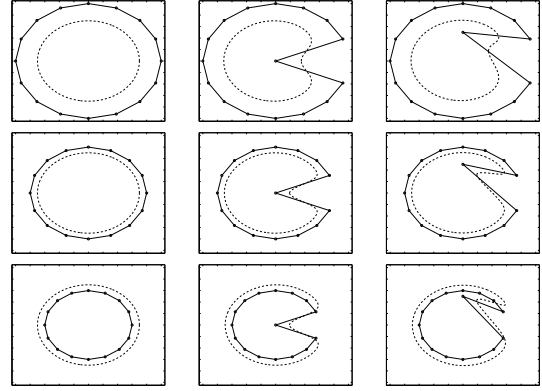


Figure 3: The curve deformation for different polygon movements: external polygon (first and second row) and internal polygon (third row). The polygon is shown as solid line and the evolving curve as dashed line.

exterior region points will be described with respect to these cage points using the affine coordinates. The cage vertices will evolve according to the minimization of an energy.

### 3 METHOD

Let us denote with  $I(\mathbf{p}) : R^m \rightarrow R$  a gray-level image, where  $m = 2$  (resp.  $m = 3$ ) refers to a two-dimensional (resp. three-dimensional) data. Let  $\mathbf{p}$  be a point of  $R^m$  and let us denote  $\mathbf{v} = \{v_1, \dots, v_N\}$  the set of cage vertices (or control points) associated to our parametrization. As commented previously, for  $m = 2$  the cage is a closed polygon whereas for  $m = 3$  the cage is a closed surface made up of triangles.

Let  $\Omega_1$  and  $\Omega_2$  be the set of pixels of the interior and exterior, respectively, of the evolving interface  $C$ . For each point  $\mathbf{p}$  of  $\Omega_1$  and  $\Omega_2$  the affine coordinates are computed. When a cage vertex  $v_i$  is moved, the points inside  $\Omega_1$  and  $\Omega_2$  are deformed accordingly (see Figure 2). Thus, in our work the evolving interface does not need to be explicitly used to determine  $\Omega_1$  and  $\Omega_2$ .

For simplicity we concentrate on the Chan and Vese model. However, the method can be easily extended to other types of models. The Chan and Vese model assumes that the gray-level values of pixels inside  $\Omega_1$  and  $\Omega_2$  can be modelled with different mean values. The energy functional to minimize is:

$$E(\mathbf{v}) = \frac{1}{|\Omega_1|} \sum_{\mathbf{p} \in \Omega_1} \frac{1}{2} (I(\mathbf{p}) - \mu_1)^2 + \frac{1}{|\Omega_2|} \sum_{\mathbf{p} \in \Omega_2} \frac{1}{2} (I(\mathbf{p}) - \mu_2)^2. \quad (10)$$

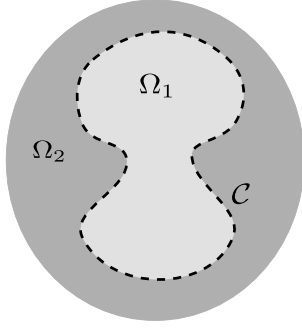


Figure 4: For a region-based energy term the contour (dashed line) is evolved by minimizing an energy measured in the interior region,  $\Omega_1$ , and the exterior region,  $\Omega_2$ . For edge-based energies the contour is evolved by minimizing an energy on the evolving interface.

where the mean gray-level value of  $\Omega_h$  with  $h \in \{1, 2\}$  is defined as

$$\mu_h = \frac{1}{|\Omega_h|} \sum_{\mathbf{p} \in \Omega_h} I(\mathbf{p}), \quad (11)$$

and  $|\cdot|$  denotes the cardinal of the set. The energy model is based on a direct discretization of the energy functional of Equation (2). In order to minimize such equation, one approach is to compute its gradient and use it to drive the evolution of the interface to the minimum. This approach is called discretized optimization approach in the context of energy minimization problems (Kalmoun et al., 2011).

Let  $\mathbf{v}_j = (v_{j,x}, v_{j,y})^T$  for  $m = 2$  (resp.  $\mathbf{v}_j = (v_{j,x}, v_{j,y}, v_{j,z})^T$  for  $m = 3$ ) be the coordinates of a cage vertex. The gradient of the energy with respect to  $v_{j,x}$  is given by

$$\frac{\partial}{\partial v_{j,x}} \frac{1}{2} (I(\mathbf{p}) - \mu_h)^2 = (I(\mathbf{p}) - \mu_h) \left( \frac{\partial I(\mathbf{p})}{\partial x} \frac{\partial \mathbf{p}}{\partial v_{j,x}} - \frac{\partial \mu_h}{\partial v_{j,x}} \right). \quad (12)$$

A similar expression is obtained for the partial derivative with respect to  $v_{j,y}$  and  $v_{j,z}$ . The partial derivatives with respect to  $\mathbf{v}_j$  can be expressed in a compact form as follows

$$\nabla_{\mathbf{v}_j} \frac{1}{2} (I(\mathbf{p}) - \mu_h)^2 = (I(\mathbf{p}) - \mu_h) (\varphi_j(\mathbf{p}) \nabla I(\mathbf{p}) - \nabla_{\mathbf{v}_j} \mu_h), \quad (13)$$

where

$$\nabla_{\mathbf{v}_j} \mu_h = \frac{1}{|\Omega_h|} \sum_{\mathbf{p} \in \Omega_h} \varphi_j(\mathbf{p}) \nabla I(\mathbf{p}). \quad (14)$$

Thus, the gradient of  $E$  can be expressed as

$$\begin{aligned} \nabla_{\mathbf{v}_j} E(\mathbf{v}) = & \frac{1}{|\Omega_1|} \sum_{\mathbf{p} \in \Omega_1} (I(\mathbf{p}) - \mu_1) (\varphi_j(\mathbf{p}) \nabla I(\mathbf{p}) - \nabla_{\mathbf{v}_j} \mu_1) \\ & + \frac{1}{|\Omega_2|} \sum_{\mathbf{p} \in \Omega_2} (I(\mathbf{p}) - \mu_2) (\varphi_j(\mathbf{p}) \nabla I(\mathbf{p}) - \nabla_{\mathbf{v}_j} \mu_2). \end{aligned}$$

Note that for the computation of the gradient we have assumed that the cardinal of sets  $\Omega_1$  and  $\Omega_2$  do not depend on the cage vertex position. Indeed, as commented before,  $\Omega_1$  and  $\Omega_2$  are made up of individual pixels that deform as the vertex positions are moved. As vertices move the corresponding evolving interface may change its length (in two dimensional problems) or area (in three dimensional problems), but in our implementation no pixels are added or removed to  $\Omega_1$  and  $\Omega_2$  as the interface evolves. This approximation may be correct if the deformation applied to the cage is not grand. If the cage deforms with a big zoom, it may be necessary to recompute, at a certain iteration, the new set of pixels  $\Omega_1$  and  $\Omega_2$ . This idea is similar to the one used in level sets implementation, in which the distance function is used for the evolving function  $\phi$ . Efficient implementations re-initialize  $\phi$  to a distance function only every certain iterations.

## 4 IMPLEMENTATION

In this Section, we describe the implementation issues associated to our proposed method.

Assume a gray-level image  $I$  and a mask  $\Omega_1$  are available. The mask  $\Omega_1$  can be for instance a binary image that is an approximation to the object we want to segment. Thus,  $\Omega_1$  will be used as initialization to our algorithm. In the case of medical images, for instance, this mask can be obtained by means of a registration of the image to be segmented with an atlas. In some cases, the mask can be manually defined by the user. In this paper we will assume that  $\Omega_1$  is a connected component. However, the method presented here is not restricted to this case. That is,  $\Omega_1$  may be composed of multiple connected components. However, note that our method is not able to deal with topological changes of  $\Omega_1$ .

Several choices are available to obtain the outer pixels  $\Omega_2$ . For instance,  $\Omega_2$  can be taken as the set  $\Omega_2 = \Omega \setminus \Omega_1$ , where  $\Omega$  is the whole image support, see Fig. 4. This is the way in which  $\Omega_2$  is defined for many level set approaches and is the case in our paper. However, other approaches are possible. For instance, only a band around  $\Omega_1$  may be taken. This is useful in order to avoid taking pixels that are too far away from

$\Omega_1$ , see (Lankton and Tannenbaum, 2008). Note that pixels of  $\Omega_1$  or  $\Omega_2$  may fall outside the polygon (2D) or surface (3D) formed by the cage vertices.

Once the set of pixels of  $\Omega_1$  and  $\Omega_2$  have been obtained, the affine coordinates of the pixels  $\mathbf{p} \in \Omega_1$  and  $\mathbf{p} \in \Omega_2$  have to be computed. The affine coordinates are computed using the cage vertices  $\mathbf{v}$  which are assumed to be given as input. Recall that for each point  $\mathbf{p} \in R^m$ ,  $m = 2$  or  $m = 3$ , a set of  $N$  coordinates (i.e. floating point values) are obtained, where  $N$  is the number of cage vertices. These coordinates only have to be computed once, before the optimization algorithm is initiated.

For a given  $E(\mathbf{v})$ , the energy is minimized using a gradient descent. The gradient method iteratively updates  $\mathbf{v}^{k+1}$  from  $\mathbf{v}^k$  as follows

$$\mathbf{v}^{k+1} = \mathbf{v}^k + \alpha \mathbf{s}^k \quad (15)$$

where  $\mathbf{s}^k$  is the so called search direction which is the negative gradient direction  $\mathbf{s} = -\nabla E(\mathbf{v}^k)$ . The step  $\alpha$  is computed via a back-tracking algorithm. Starting with an  $\alpha = \alpha_0$ , the algorithm iteratively computes  $E(\mathbf{v}^k + \alpha \mathbf{s}^k)$  and reduces  $\alpha$  until  $E(\mathbf{v}^k + \alpha \mathbf{s}^k) < E(\mathbf{v}^k)$ .

The computation of  $\alpha_0$  is a critical issue for good performance of the algorithm. In this paper  $\alpha_0$  is automatically computed at each iteration  $k$  so that the cage vertices move at most  $\beta$  pixels from its current position. That is,

$$\alpha_0 = \max_{\alpha} \{ \alpha \mid \|\mathbf{v}_j^{k+1} - \mathbf{v}_j^k\| \leq \beta \} \quad j = 1 \dots N \quad (16)$$

where  $\beta$  is a user given parameter (usually set to 5 in the experiments). The backtracking algorithm iteratively reduces the value of  $\alpha$  until a value of  $\alpha$  that decreases the energy value is found. The gradient descent stops when the backtracking reduces the  $\alpha$  below a threshold associated to a cage movement, for instance 0.05 pixels.

For a given  $\mathbf{v}$ , the corresponding ‘‘deformed’’ pixel positions  $\mathbf{p}$  of  $\Omega_1$  and  $\Omega_2$  are recovered using (9). The energy  $E(\mathbf{v})$  and gradient  $\nabla E(\mathbf{v})$  can be then computed. Note that the recovered pixel positions  $\mathbf{p}$  may be non-integer positions. Hence, we apply linear interpolation to estimate  $I(\mathbf{p})$  and  $\nabla I(\mathbf{p})$  at such points. In addition, those pixels that fall outside of the image support are back projected to the image border (i.e. pixels at the image border are assumed to extend to infinity).

To recover the final position of the interface we parametrize the interface at the beginning (before optimization starts) with respect to the cage vertices. After convergence, the resulting interface can be easily recovered by using Equation (9).

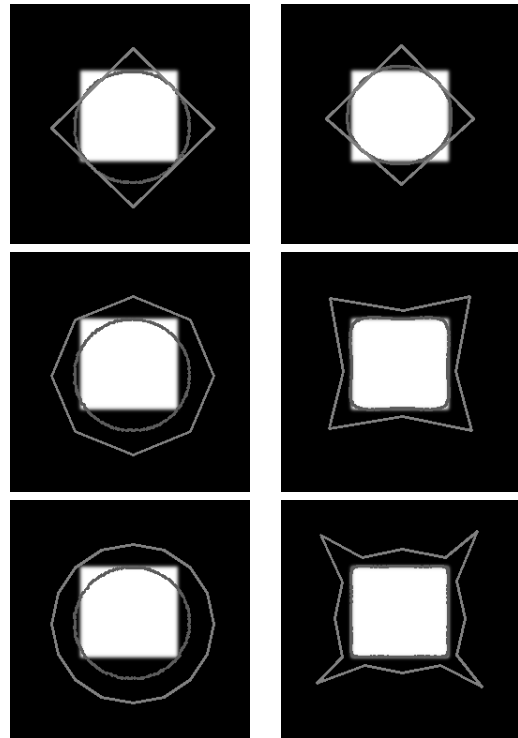


Figure 5: Results for a synthetic image using different number of cage points. Top, 4 cage points. Middle, 8 cage points. Bottom, 16 cage points. On the left column the initial images are shown, while the right correspond to the results.

## 5 EXPERIMENTAL RESULTS

In this section we present the experimental results for two and three dimensional segmentation problems. In particular, we perform different experiments to show different characteristics of the proposed segmentation method: the influence of the number of cage vertex selection, the importance of the cage shape, and the performance on some real images.

### 5.1 Two dimensional segmentation

We begin with the two dimensional segmentation, that is, the image  $I : R^2 \rightarrow R$ . We consider first some synthetic images, namely a square and a star, to analyze the behaviour of our approach. For these experiments  $\Omega_1$  is taken to be the whole interior of the evolving interface and  $\Omega_2$  the whole exterior. We would like to point out that in order to generate these images the cage and the evolving contour has been painted rounding the coordinates to nearest integers. Thus, within the resulting images shown in this section there may seem to be noisy boundaries.

Figure 5 is devoted to show the influence of the

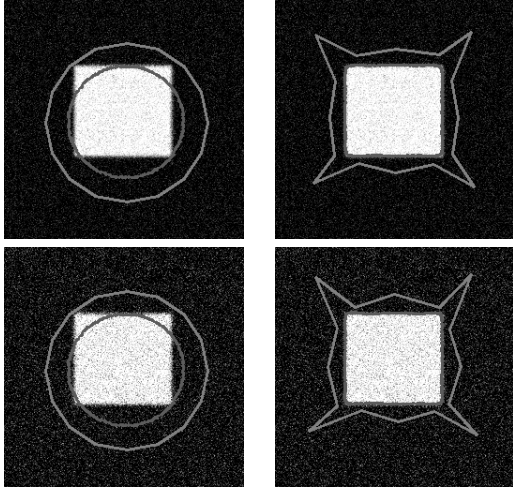


Figure 6: Results for a synthetic image and 16 cage points using different levels of Gaussian noise. Top, noise variance is  $\sigma^2 = 0.3$ . Bottom,  $\sigma^2 = 0.5$ , where the image gray-level is assumed to be normalized to the range  $[0, 1]$ .

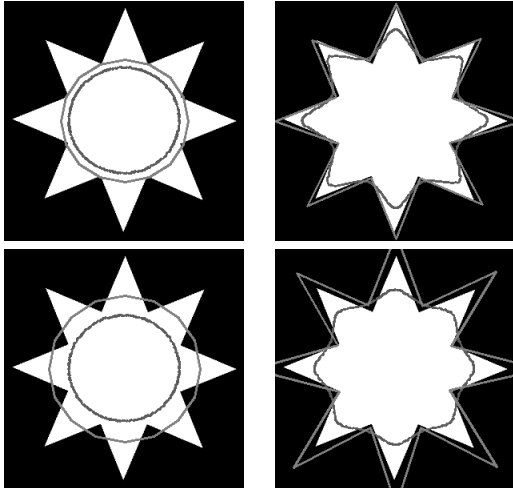


Figure 7: Results for a synthetic image with cages at different distances from the evolving contour. Images on the left are the initial images and on the right are corresponding results.

number of cage points to the segmentation result. The initializations are shown on the left column and the resulting segmentations are shown on the right. The cages are drawn with light gray whereas the evolving interface with dark gray. Experiments show how the interface deforms when using 4, 8 and 16 cage points. As can be seen, increasing the number of cage points allows better adaptation to the shape of the object of interest. The number of cage points influences the regularization of the evolving contour.

Figure 6 shows the robustness of the method to simple Gaussian noise. As expected, the model pro-

posed in Equation (10) is robust to Gaussian noise.

Figure 7 shows the effect of the cage distance to the evolving interface. For both experiments the initial evolving interfaces are the same, but the cages are created at a different distance from the evolving interface: the distance on the top is smaller than the bottom. The images on the left show initializations, whereas the images on the right show the results. It can be observed that the distance between the evolving interface and the cage plays an important role in the deformations that can be applied to the evolving interface. In addition, note that the result is inherently regular (smooth ends instead of sharp ends) due to the nature of the parametrization. Therefore no regularization terms are needed in the energy function.

We now show results on real images. We have compared our method with a level-set based Chan and Vese implementation available in (Getreuer, 2012). The code implements the following energy

$$E(C) = \mu \text{Length}(C) + \nu \text{Area}(C) + \lambda_1 \frac{1}{2} \iint_{\Omega_1} (I - \mu_1)^2 dx dy + \lambda_2 \frac{1}{2} \iint_{\Omega_2} (I - \mu_2)^2 dx dy. \quad (17)$$

The first term of this energy controls the regularity of the evolving contour  $C$  by penalizing the length. The second term penalizes the enclosed area of  $C$  to control its side. The third and fourth terms are the terms we use in our energy and penalize the discrepancy between the piecewise constant models  $\mu_1$  and  $\mu_2$  and the input image.

The previous energy is implemented by means of a level-set, please see details in (Getreuer, 2012). As an example, we show in Figure 8 a segmentation result. The initialization of the level-set is performed by using a checkerboard shape and is shown in the middle Figure. The resulting segmentation is shown in white on the right Figure and has been obtained with the parameters  $\mu = 0.25$ ,  $\nu = 0.0$ ,  $\lambda_1 = 1.0$  and  $\lambda_2 = 1.0$ . As can be seen, level-set based methods are able to deal with topology changes and thus multiple connected components may be obtained in the segmentation. Observe that here two contours have been obtained as result: the contour around the elephant and the one (small circle) over the head of the elephant.

The results for the same image and two other real images are shown in Figure 9. On the left, the initialization is shown: the cage is drawn in black color and the initial evolving contour in white. In the middle, the resulting segmentation obtained with our method is shown. On the right, the segmentation obtained with the Chan and Vese level-set method is shown.

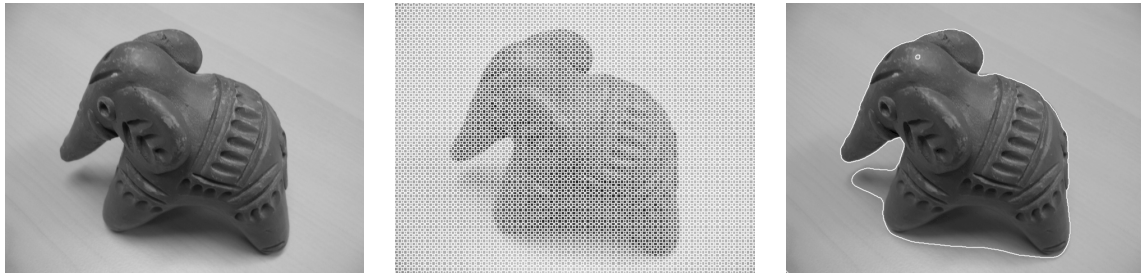


Figure 8: Example of level-set Chan and Vese segmentation. On the left, original image is shown. Initialization, a checker board shape for the embedded function, is shown in the middle. On the right, resulting segmentation shows contour in white color.

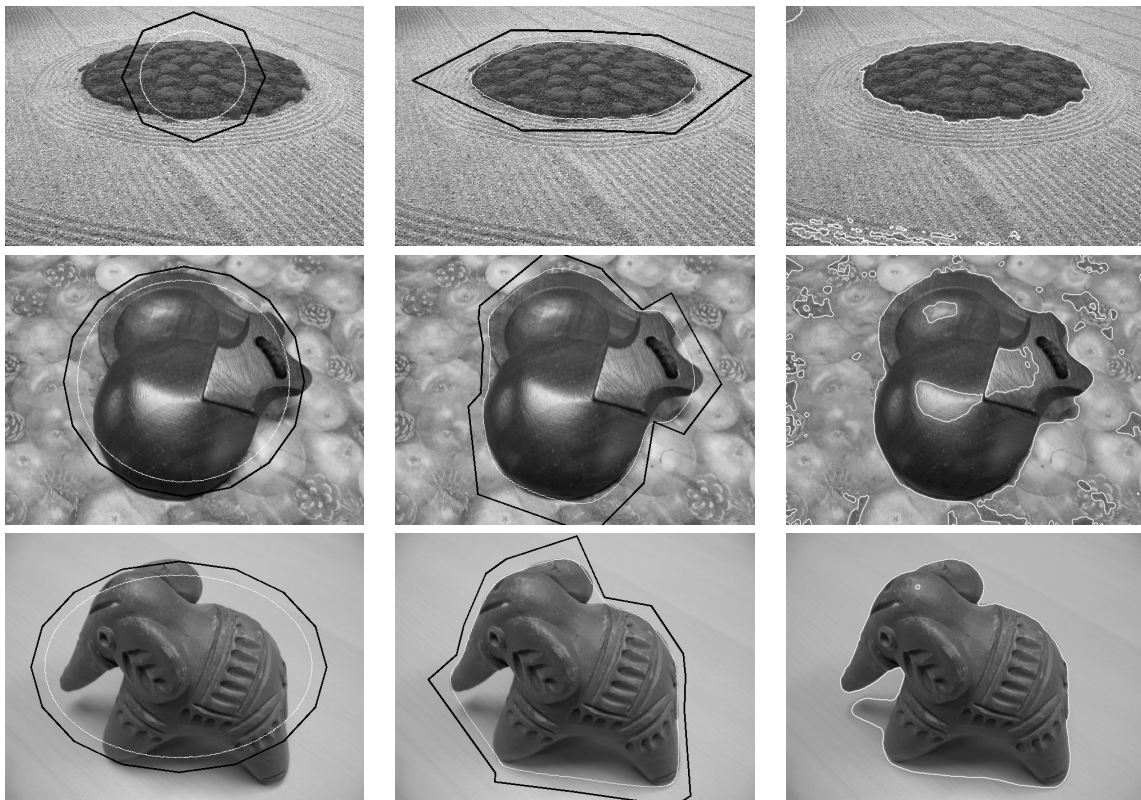


Figure 9: Results for some real images. On the left column, the initialization is shown: the cage is drawn in black color whereas the evolving contour in white color. From top to bottom, the number of cage vertices used is 8, 16 and 16. In the middle, the resulting segmentation obtained with our method is shown: the resulting cage and segmentation are again shown in black and white, respectively. On the right, the resulting segmentation using a level-set based Chan and Vese segmentation is shown.



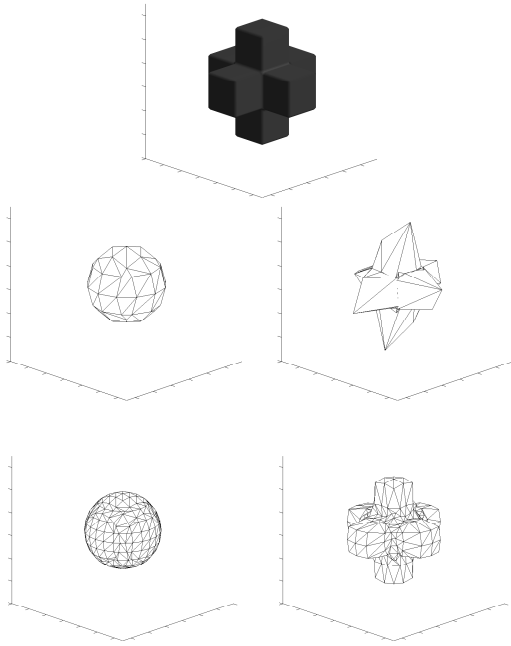


Figure 10: Results for a synthetic 3D image. Top, original binary image. Middle left, the initial surface. The cage has the same number of triangles but has a slightly higher radius. Middle right, resulting surface after evolution. Bottom, the same experiment is repeated but with a higher number of triangles for both the initial surface and the cage.

The parameters that have been used for the latter are  $\mu = 0.25$ ,  $\nu = 0.0$ ,  $\lambda_1 = 1.0$ ,  $\lambda_2 = 1.0$  for the second and third row, whereas  $\mu = 0.1$ ,  $\nu = 0.0$ ,  $\lambda_1 = 1.0$ ,  $\lambda_2 = 1.0$  has been used for the first row.

As can be seen, our method is able to obtain a regular boundary without using any specific energy term. Regularization is obtained thanks to the used parametrization. In the level-set method, regularization has to be explicitly introduced in the energy term. On the other hand, the level-set method is able to deal with topology changes (see the rather high number of regions obtained in the images on the right column), whereas our method does not. As commented before, this limitation is a mild constraint in many applications, where the goal may be to simply segment one connected object and thus the topological flexibility of the level sets is not needed.

## 5.2 Three dimensional segmentation

We now show some examples for the three dimensional segmentation problem. As commented before, in this case the cage is a surface made up of triangles.

Figure 10 shows an example for a synthetic image. The original image is shown on the top of the

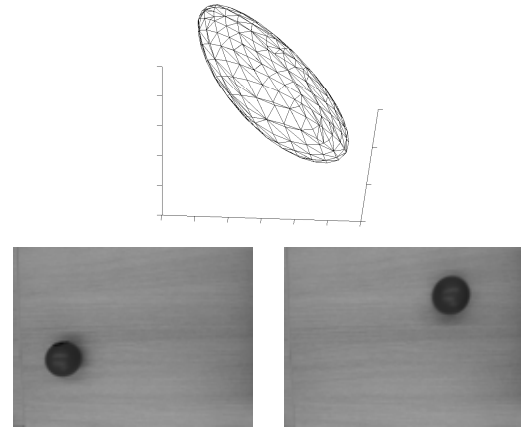


Figure 11: Result for a real 3D image. Bottom, two of the images of the video. Video images a stacked to form a 3D image. Top, segmentation result for the moving ball.

Figure and represents a binary image with a cross. The original surface is a ball which constructed using the marching cube algorithm, is drawn on the middle left. The cage is created from the previous surface just by inflating it a bit (0.5 pixels). The surface is then evolved using the proposed energy and the resulting segmentation is drawn on the middle right. At the bottom the same experiment is shown but in this case the cage (as well as the mask) are modelled with a higher number of vertices. As can be seen, the number of vertices plays an important role in order to adapt the evolving surface to the object of interest.

Finally, we show the result with real images, see Figure 11. We have recorded a video in which a ball moves along a line. The initial and end position of the ball is shown on the bottom. The individual images of the video are then stacked as a 3D image, and an initial mask is created by defining a 3D ball whose center is approximately at the middle point joining the initial and end position and whose radius (in 3D) is the radius of the moving ball. On the top of Figure 11, it can be seen the result after convergence has reached. As can be observed, our method is able to properly extract the “shape” of the 3D object formed by the moving ball.

## 5.3 Computation time

Currently, the code for 2D has been implemented in C language whereas the 3D only has been implemented in MATLAB. Regarding the 2D segmentation, the total amount of time spend by the algorithm is less than one minute. This includes the computational time of the mean value coordinates for all pixels of the im-

age and the gradient descent to evolve the contour. With respect the 3D segmentation, the bottleneck is currently at the computation of the mean value coordinates for all the voxels of the volume, which may take a long time. Gradient descent takes then about a minute to converge.

Our method can be easily parallelized. Indeed, two issues use most of the computation resources in our approach, namely the interpolation of the image at non-integer values (see Equation (9)) and the computation of the mean value coordinates. These two issue will receive our focus of attention in future work.

## 6 CONCLUSIONS

In this paper, we have presented a parametrized active contour approach for both two and three dimensional segmentation problem. In our method the interface is evolved by moving a set of cage points. In the two dimensional problem the cage is a closed polygon whereas in the three dimensional problem the cage is a closed surface (made up of triangles). Mean value coordinates are used to parametrize the points of the space, inside or outside the cage. Other parametrization possibilities exist (such as harmonic coordinates or Green coordinates), but we have selected mean value coordinates since they are simple to compute compared to other methods. Note that the parametrization has an intuitive interpretation. By moving a cage point, the associated points are moved correspondingly. This allows to introduce into the segmentation process the user interactivity: the user may, for instance, manually move the control points to the correct position so that the system automatically learns from them.

In addition, within our framework, the regularization of the evolving interface can be controlled via the cage itself: the larger the distance of the cage to the evolving contour, the higher the contour regularization. Thus, there is really no need to include regularization terms within the energy.

Our framework is suitable for the implementation of discrete energies, both region-based and edge-based terms, although we have shown here only the application to a region-based energy, namely the classical Chan and Vese one.

Morover, we think that our method can be easily embedded in a shape-constrained approach, that is, an approach in which the movement of the cage is constrained so as to ensure certain shapes for the evolving contour. Our future work is to apply our method for 3D medical image segmentation problems and parallelize the method to improve its speed.

## ACKNOWLEDGEMENTS

Q. Xue would like to acknowledge support from Erasmus Mundus BioHealth Computing, L. Igual and L. Garrido by MICINN projects, reference TIN2012-38187-C03-01 and MTM2012-30772 respectively.

## REFERENCES

- Barbosa, D., Diertenbeck, T., Schaerer, J., D'hooge, J., Friboulet, D., and Bernard, O. (2012). B-spline explicit active surfaces: an efficient framework for real-time 3D region-based segmentation. *IEEE Transactions on Image Processing*, 21(1):241–251.
- Caselles, V., Kimmel, R., and Sapiro, G. (1997). Geodesic active contours. *International Journal of Computer Vision*, 22:61–79.
- Chan, T. and Vese, L. (2001). Active contours without edges. *IEEE Trans. on Imag. Proc.*, 10(2):266–277.
- Coquillart, S. (1990). Extended free-form deformation: a sculpturing tool for 3d geometric modeling. *SIGGRAPH*, 24(4):187–196.
- Faloutsos, P., van de Panne, M., and Terzopoulos, D. (1997). Dynamic free-form deformations for animation synthesis. *IEEE Transactions on Visualization and Computer Graphics*, 3(3):201–214.
- Floater, M. S. (2003). Mean value coordinates. *Computer Aided Geometric Design*, 20(1):19–27.
- Getreuer, P. (2012). Chan-veese segmentation. *Image Processing On Line*.
- Gouraud, H. (1971). Continuous shading of curved surfaces. *IEEE Transactions on Computers*, C-20(6):623 – 629.
- Hormann, K. and Floater, M. (2006). Mean value coordinates for arbitrary planar polygons. *ACM Transactions on Graphics*, 25(4):1424–1441.
- Hormann, K. and Greiner, G. (2000). Continuous shading of curved surfaces. *Curves and Surfaces Proceedings (Saint Malo, France)*, pages 152 – 163.
- Jacob, M., Blu, T., and Unser, M. (2004). Efficient energies and algorithms for parametric snakes. *IEEE Transactions on Image Processing*, 13(9):1231–1244.
- Joschi, P., Meyer, M., DeRose, T., Green, B., and Sanocki, T. (2007). Harmonic coordinates for character articulation. In *SIGGRAPH*.
- Ju, T., Schaefer, S., and Warren, J. (2005). Mean value coordinates for closed triangular meshes. In *Proceedings of ACM SIGGRAPH*, volume 24, pages 561–566.
- Kalmoun, M., Garrido, K., and Caselles, V. (2011). Line search multilevel optimization as computational methods for dense optical flow. *SIAM Journal of Imaging Sciences*, 4(2):695–722.
- Kass, M., Witkin, A., and Terzopoulos, D. (1988). Snakes: Active contour models. *International Journal of Computer Vision*.

- Lankton, S. and Tannenbaum, A. (2008). Localizing region-based active contours. *IEEE Transactions on Image Processing*, 17(11):2029–2039.
- Lipman, Y., Kopf, J., Cohen-Or, D., and Levin, D. (2007). GPU-assisted positive mean value coordinates for mesh deformations. In *Eurographics Symposium on Geometry Processing*.
- Lipman, Y., Levin, D., and Cohen-Or, D. (2008). Green coordinates. In *SIGGRAPH*.
- Michailovich, O., Rathi, Y., and Tannenbaum, A. (2007). Image segmentation using active contours driven by the Bhattacharyya gradient flow. *IEEE Transactions on Image Processing*, 16(11):2787–2801.
- Rousson, M. and Deriche, R. (2002). A variational framework for active and adaptative segmentation of vector valued images. In *Proceedings of the Workshop on Motion and Video Computing*, pages 56–61. IEEE Computer Society.
- Rueckert, D., Sonoda, L., Hayes, C., Hill, D., Leach, M., and Hawkes, D. (1999). Nonrigid registration using free-form deformations: application to breast MR images. *IEEE Transactions on Medical Imaging*, 18(8):712–721.